Communications in Statistics—Theory and Methods, 34: 163–192, 2005

ISSN: 0361-0926 print/1532-415X online
DOI: 10.1081/STA-200045869

Time Series Analysis

Nonstationary Data Analysis by Time Deformation

HENRY L. GRAY, CHU-PING C. VIJVERBERG, AND WAYNE A. WOODWARD

Southern Methodist University, Dallas, Texas, USA

In this article we discuss methodology for analyzing nonstationary time series whose periodic nature changes approximately linearly with time. We make use of the M-stationary process to describe such data sets, and in particular we use the discrete Euler(p) model to obtain forecasts and estimate the spectral characteristics. We discuss the use of the M-spectrum for displaying linear time-varying periodic content in a time series realization in much the same way that the spectrum shows periodic content within a realization of a stationary series. We also introduce the instantaneous frequency and spectrum of an M-stationary process for purposes of describing how frequency changes with time. To illustrate our techniques we use one simulated data set and two bat echolocation signals that show time varying frequency behavior. Our results indicate that for data whose periodic content is changing approximately linearly in time, the Euler model serves as a very good model for spectral analysis, filtering, and forecasting. Additionally, the instantaneous spectrum is shown to provide better representation of the time-varying frequency content in the data than window-based techniques such as the Gabor and wavelet transforms. Finally, it is noted that the results of this article can be extended to processes whose frequencies change like at^{α}, $a > 0$, $-\infty < \alpha < -\infty$.

Keywords Euler processes; M-stationary processes; Nonstationary; Time deformation.

Mathematics Subject Classification Primary 62M10: times series, auto-correlation, regression, etc; Secondary 62M15: spectral analysis.

1. Introduction

Gray and Zhang (1988) introduced continuous M-stationary processes for the purpose of analyzing and forecasting nonstationary data that exhibited long memory characteristics. M-stationary processes were shown to maintain the properties of regular stationary processes if the composition law is multiplication rather than addition. For example, for M-stationary processes, $E[(X(t)X(t\tau)] = R_X(\tau)$ rather than $E[X(t)X(t+\tau)] = R_X(\tau)$. After developing the properties of

Received October 14, 2003; Accepted February 2, 2004
Address correspondence to Henry L. Gray, Southern Methodist University, USA; E-mail: hgray@mail.smu.edu

M-stationary processes, Gray and Zhang (1988) identified a number of such processes and demonstrated that for certain types of data, an M-stationary process could improve the forecasts over those obtained using usual techniques. The most extensive class of M-stationary processes studied by Gray and Zhang (1988) was the continuous "Euler Process", shown to be the M-stationary analog of continuous autoregressive processes. Unfortunately, due to the fact that they only studied the continuous case, they did not apply the Euler model to data. This has remained a barrier to the application of the Euler process, and although the process has remained of some theoretical interest (Girardin and Senoussi, 2003; Girardin and Rachdi, 2003), until now it has not been applied to data.

Recently, Vijverberg and Gray (2003) introduced the discrete Euler process as the discretization of the continuous Euler process. In that paper they introduced the concept of a dual discrete process and showed that the dual of a discrete Euler process is a discrete autoregressive process. The basic properties of a discrete Euler process were then developed and it was shown that discrete and continuous Euler processes whose characteristic equations have complex roots can be described as processes whose periodic structure is linearly changing in time. For such a process, it was shown that one could transform the process to a stationary process by sampling correctly. Several examples were given that demonstrated the applications of discrete Euler processes.

In order to characterize the changing periods and frequencies of the process, Gray and Zhang (1988) and Vijverberg and Gray (2003) introduced the concept of an M-autocorrelation and M-spectrum. Vijverberg and Gray (2003) used the M-spectrum to detect the presence of changing cycles in data, and they applied the discrete Euler model to economic data.

Even though Vijverberg and Gray (2003) developed the properties of a discrete Euler process and introduced several new concepts, they did not apply the methodology to forecasting, spectral analysis, or filtering and only considered a few economic time series. In this article we give a quick review of the necessary results from Vijverberg and Gray (2003). We then develop a forecasting and spectral analysis methodology for discrete M-stationary processes. The results are applied to real and simulated data to demonstrate that the method significantly outperforms autoregressive and window-based methods when the periodic structure is changing even approximately linearly in time.

Standard spectral analysis of a signal whose frequency is changing in time will typically result in a spectrum with many small peaks in an attempt to describe the ever-changing periodic behavior of the series. To address this problem we introduce the instantaneous spectrum of an M-stationary process as a new tool for describing the spectral behavior of data with time-varying frequencies that change like $(a + bt)^{-1}$. We demonstrate the application of the M-spectrum and the instantaneous spectrum to several simulated data sets as well as to bat echolocation data.

The question of how one can tell if an M-stationary process is an appropriate model for a given data set is addressed briefly. It is also noted that the method of time transformation is much more general than simply linearly changing periods, the M-stationary case, but in fact can be applied to any process whose frequencies change monotonically with time. Examples of work currently being completed include $G(\lambda)$ processes, which are processes whose frequencies change like $\alpha t^{-\beta}$ (see Jiang et al., 2003), including linear and quadratic chirps. Similar results can be given for exponential chirps.

2. M-Stationary and Euler Processes

2.1. *Continuous Case*

Gray and Zhang (1988) define a stochastic process $\{X(t); t \in (0, \infty)\}$ to be multiplicative stationary (M-stationary) if the following hold:

(i) $E(X(t)) = \mu$
(ii) $\mathrm{Var}(X(t)) = \sigma^2 < \infty$
(iii) $E((X(t) - \mu)(X(t\tau) - \mu)) = R_X(\tau)$.

We refer to $R_X(\tau)$ as the M-autocovariance, and it is clear that $\mathrm{Var}(X(t)) = R_X(1)$. Also, if the index set is changed from $(0, \infty)$ to $(-\infty, \infty)$ and $t\tau$ is replaced by $t + \tau$, then it is easily seen that the conditions above become the classical conditions defining a weakly stationary process. Gray and Zhang (1988) show that the time series $\{Y(u); u \in (-\infty, \infty)\}$, defined by $Y(u) = X(t)$ where $t = e^u$ is stationary if and only if $X(t)$ is M-stationary. The process $Y(u)$ is referred to as the dual of $X(t)$. Thus, if "time" is transformed (or deformed) by a logarithmic transformation, then the M-stationary process $X(t)$ becomes a classical stationary process $Y(u)$, where $u = \ln t$. It is useful to note that similar results can be obtained by letting $t = h^u$ and letting $X(t) = Y(u)$, where $u = \ln t / \ln h$ and $h > 1$ is a constant. As we will see, there is some utility in this approach especially in the discrete case. On the other hand, if $Y(u)$ is a classical stationary process, and if "time" is transformed by an exponential, then $Y(u)$ is transformed to an M-stationary process $X(t)$. Additionally, $R_X(\tau) = C_Y(\ln \tau)$ for $\tau > 0$ where $C_Y(w)$ denotes the usual autocovariance, at lag w, of the stationary process $Y(u)$. Gray and Zhang (1988) also define the M-spectrum of the M-stationary process $X(t)$ to be the Mellin transform $G_X(f) = \int_0^\infty \tau^{-2\pi i f - 1} R_X(\tau) d\tau$, and they show that $G_X(f) = S_Y(f)$ where $Y(u)$ is the dual of $X(t)$ and where $S_Y(f)$ denotes the usual spectrum of the stationary process $Y(u)$.

An example of an M-stationary process is the kth order continuous Euler process defined by Gray and Zhang (1988) as a process satisfying

$$t^k X^{(k)}(t) + \psi_1 t^{k-1} X^{(k-1)}(t) + \cdots + \psi_k (X(t) - \mu) = \varepsilon(t), \tag{2.1}$$

where $\varepsilon(t)$ is M-white noise (see Gray and Zhang, 1988), $E(\varepsilon(t)) = 0$, and the ψ_i are constants. The dual process, $Y(u)$, of the kth order continuous Euler process, $X(t)$, is the kth-order continuous auto regressive (AR) process

$$Y^{(k)}(u) + \phi_1 Y^{(k-1)}(u) + \cdots + \phi_k (Y(u) - \mu) = \eta(u), \tag{2.2}$$

where the φ_i's are constants determined by the ψ_i's and where $\eta(u)$ is continuous white noise. It should be noted that the coefficients of the continuous Euler models vary with time while the coefficients of the continuous AR models are constant values. If $X(t)$ is a kth order continuous Euler process, the autocovariance, $C_Y(w)$, of the dual process $Y(u)$ satisfies a homogenous differential equation with constant coefficients. If the characteristic equation of the dual has $2q$ complex roots (suppose, for ease of notation, none are repeated), then the corresponding terms in $C_Y(\tau)$ are of the form

$$\sum_{j=1}^{q} \left[c_j e^{a_j \tau} \cos(b_j \tau) + d_j e^{a_j \tau} \sin(b_j \tau) \right], \quad \tau > 0 \tag{2.3}$$

while the corresponding terms in $R_X(\tau)$ are of the form

$$\sum_{j=1}^{q} \left[c_j \tau^{a_j} \cos(b_j \ln \tau) + d_j \tau^{a_j} \sin(b_j \ln \tau) \right], \quad \tau > 1, \tag{2.4}$$

where a_j is the real part of the jth complex root and b_j is the imaginary part.

2.2. *Discrete Case*

Vijverberg and Gray (2003) extend the concept of an M-stationary process to the discrete case. For more details concerning discrete M-stationary processes see Vijverberg (2002). Let $h > 1$ and $S = \{t : t = h^k, k = 0, \pm 1, \pm 2, \dots\}$. Then Vijverberg and Gray (2003) define $X(t)$, $t \in S$ to be a discrete M-stationary process if the following conditions hold:

(i) $E(X(t)) = \mu$
(ii) $\mathrm{Var}(X(t)) < \infty$
(iii) $E((X(t) - \mu)(X(t\tau) - \mu)) = R_X(\tau)$

for all t and $t\tau \in S$. Additionally, Vijverberg and Gray (2003) define the dual of X_t by $Y_k = X(h^k)$, $k = 0, \pm 1, \pm, \dots$, and show that $C_Y(k) = R_X(h^k)$. It follows directly that $R_X(h^\tau) = R_X(h^{-\tau})$ and that $\{X(t)\}$ is discrete M-stationary if and only if $\{Y_k\}$ is stationary. Vijverberg and Gray (2003) define the discrete M-spectrum, $G_X(f^*)$, as the discrete Mellin transform

$$G_X(f^*) = \sum_{k=-\infty}^{\infty} h^{-2\pi i f^* k} R_X(h^k), \tag{2.5}$$

where $h > 1$, $|f^* \ln h| \leq 1/2$, and f^* is referred to as M-frequency. They show that $G_X(f^*) = S_Y(f)$, where $|f| = |f^* \ln h| < 1/2$, $G_X(f^*)$ is the M-spectrum of $X(t)$, and $S_Y(f)$ is the usual spectrum of the dual process Y_k. Thus, the M-spectrum, $G_X(f^*)$, and the spectrum of the stationary dual, i.e., $S_Y(f)$, have the same shape and differ only with respect to the "frequency" scale. It should be noted that $|f^*| \leq 1/(2 \ln h)$ so that for f measured in cycles/sampling unit, we call $1/(2 \ln h)$ the "M-Nyquist" frequency. Thus, for a given h, it follows that $1/(2 \ln h)$ is the highest M-frequency that can be detected. More generally, if the dual is sampled at units of $k\Delta$, then the M-Nyquist frequency is $1/(2\Delta \ln h)$.

The time transformation required to move from the original time scale to that of the dual process is $k = \ln t / \ln h$ where $t = h^k$ is the original variable. This is analogous to the time transformation $u = \ln t$ (or, as mentioned previously, $u = \ln t / \ln h$) in the continuous case. Thus one would expect that a continuous M-stationary process can be approximately transformed to a discrete stationary dual process by sampling in increments of h^k so that $Y_k = X(h^k)$. Of course, most time series data are collected at equally spaced increments. Thus, it will usually be necessary to interpolate to obtain values at the time points $h^1, h^2, \dots, h^n$ in order to estimate the dual process. This will be discussed in more detail in Sec. 6.

To be specific, let $t \in S$ where $S = \{t : t = h^k, k = 0, \pm 1, \pm 2, \dots\}$. Then Vijverberg and Gray (2003) define $X(t)$ to be a discrete pth order Euler process if

$X(t)$ is the M-stationary solution of

$$(X(t)-\mu)-\phi_1\left(X\left(\frac{t}{h}\right)-\mu\right)-\phi_2\left(X\left(\frac{t}{h^2}\right)-\mu\right)$$
$$-\cdots-\phi_p\left(X\left(\frac{t}{h^p}\right)-\mu\right)=a(t), \tag{2.6}$$

where $a(t)$ is white noise and $h>1$. They showed that taking the limit as $h\to 1$ in (2.6) gives the continuous AR(p) process

$$t^pX^{(p)}(t)+\psi_1t^{p-1}X^{(p-1)}(t)+\cdots+\psi_pX(t)=Z(t),$$

where the ψ_i's are functions of the ϕ_i's and where $Z(t)$ is M-white noise. Thus, in the limit, $\{X(t)\}$ is a pth order continuous Euler process. If we let $t=h^k$ and without loss of generality we let $\mu=0$, then (2.6) becomes

$$X(h^k)-\phi_1X(h^{k-1})-\phi_2X(h^{k-2})-\cdots-\phi_pX(h^{k-p})=a(h^k). \tag{2.7}$$

It follows directly that $\{X(t)\}$ in (2.7) is a pth order discrete Euler process if and only if its dual process $\{Y_k : k=0,\pm1,\dots\}$ is the autoregressive process

$$Y_k-\phi_1Y_{k-1}-\cdots-\phi_pY_{k-p}=z_k \tag{2.8}$$

where $z_k=a(h^k)$. It should be noted that the coefficients of the discrete pth order Euler model are the same as the coefficients of the discrete AR(p) model for the dual process. Thus, estimates of the parameters of the discrete pth Euler model are obtained by finding the corresponding parameter estimates of the dual AR(p) model. If $X(t)$ is a discrete Euler process, then in place of (2.3) and (2.4), we have

$$\sum_{k=1}^{q}r_k^{-\tau}\left[c_k\cos(\beta_k\tau)+d_k\sin(\beta_k\tau)\right],\quad \tau=1,2\dots \tag{2.9}$$

and

$$\sum_{k=1}^{q}(r_k^{-1/\ln h})^{\ln h^\tau}\left[c_k\cos\left(\frac{\beta_k}{\ln h}\ln h^\tau\right)+d_k\sin\left(\frac{\beta_k}{\ln h}\ln h^\tau\right)\right], \tag{2.10}$$

respectively where $r_k=\sqrt{a_k^2+b_k^2}$, $\beta_k=\arctan\frac{b_k}{a_k}$ and a_k is the real part of the kth complex root and b_k is the imaginary part. We will refer to r_k and $\beta_k/2\pi$ as magnitude and frequency, respectively.

The M-power spectrum of the pth order discrete Euler process $\{X(t)\}$ is defined to be

$$G_X(f^*)=\frac{\sigma_a^2}{|\phi(e^{-2\pi if^*\ln h})|^2}$$
$$=\frac{\sigma_a^2}{|1-\phi_1e^{-2\pi if^*\ln h}-\phi_2e^{-4\pi if^*\ln h}-\cdots-\phi_pe^{-2p\pi if^*\ln h}|^2}, \tag{2.11}$$

and the M-spectral density is

$$g(f^*) = \frac{\sigma_a^2}{\sigma_X^2 |\phi(e^{-2\pi i f^* \ln h})|^2}. \tag{2.12}$$

By replacing the parameters in (2.11) and (2.12) by estimates, we obtain the Euler spectrum and spectral density estimators, respectively. These spectral estimators have the dual relationship observed previously in that the Euler spectral estimator and the dual AR spectral estimator differ only in scale. The sample M-spectrum and the dual sample spectrum have the same relationship.

3. Origin Offset/Realization Offset

The correlation function of a stationary process is, of course, not a function of time, while the correlation function of an M-stationary process does change with time. (The M-correlation is not a function of time, but the correlation is.) The impact of this, from a data point of view, is that in order to properly model a discrete M-stationary process, one needs some estimate of the location of the initial observation. This differs from the case of stationary discrete processes where without loss of generality the origin of the observations can always be taken as zero and the observations can be considered to be taken at $k\Delta$, $k = 1, \ldots, n$. Thus, the initial observation is at Δ and without loss of generality, we usually take $\Delta = 1$.

In the discrete M-stationary case, the observations are taken at h^{j+k} where h^j is the origin for the observations. The initial observation is then taken at h^{j+1}. However, neither h nor h^j is known, so they must be selected from the data. Since the M-stationary process origin is at zero, we shall refer to h^j as the "origin offset" or the "realization offset."

Figure 1 shows a realization of length $n = 500$ from the discrete Euler(2) process

$$X(h^k) - 1.732X(h^{k-2}) + .98X(h^{k-2}) = a(h^k) \tag{3.1}$$

with $h^j = 20$ and $h = 1.01$. We now compare the first 100 observations with the last 100 observations. Clearly, as will always be the case with M-stationary data, the initial 100 points are of higher frequency than the last 100 points. Although we have not discussed how h is selected, we will later see that if the first 100 points of this realization are used as our data set, then the best choice of h will not be the same as the best choice of h if only the last 100 points are used as our data. Thus, given a realization, we generally will need to select h and the origin offset h^j.

4. Instantaneous Frequency and Instantaneous Spectrum

In Sec. 2 we defined the M-frequency and M-spectrum. In this section we discuss these concepts in more detail and relate these concepts to the instantaneous frequency and spectrum. We will subsequently show that the instantaneous spectrum is a very useful tool for displaying time-varying frequency behavior. In the classical sense, a function is said to be periodic with period (or cycle length) Δ over a set I if Δ is the minimum value in I such that $g(t) = g(t + \Delta)$ for all $t \in I$. In this case, the corresponding frequency, f, is $1/\Delta$. The following definition extends this notion to the M-periodic setting.

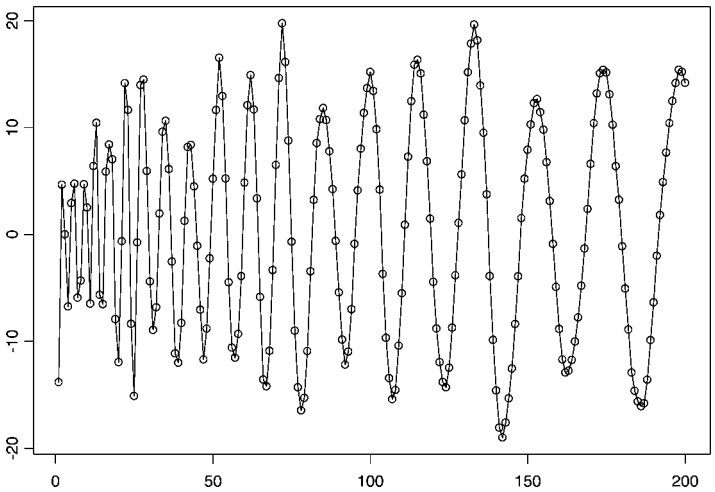

Figure 1. Realization from the Euler(2) model in (3.1).

Definition 4.1. A function, $g(t)$, is M-periodic over I with multiplicative period (i.e., M-period) δ, if $\delta > 1$ is the minimum value of $\delta \in I$ such that $g(t) = g(t\delta)$ for all $t \in I$. The associated M-frequency, f^*, is defined as $f^* = (\ln \delta)^{-1}$.

As an example consider $g(t) = \cos \beta \ln t$. In this case, $\delta = e^{2\pi/\beta}$ since $g(t\delta) = \cos \beta \ln(te^{2\pi/\beta}) = \cos(\beta \ln t + 2\pi) = g(t)$. Also, $f^* = \beta/(2\pi)$. From the definition, it follows that for each fixed t, an M-periodic function returns to the value $g(t)$ at the distance $t\delta - t = t(\delta - 1)$. Thus, when viewed on a "regular time" scale, $g(t)$ has periods that lengthen linearly.

The M-spectrum has the same role as the traditional spectrum in reflecting the most important M-periodic components in the data. However, given an M-stationary time series X_t, the traditional spectrum and the M-spectrum are not the same. Because frequencies in an M-stationary process change with time, usual spectral estimators will generally find poorly defined peaks or many peaks in an attempt to characterize this behavior if the change is significant. This will be illustrated via examples.

In the discrete setting, Vijverberg and Gray (2003) define the instantaneous period of an M-periodic function at time h^k to be

$$P(h^k; f^*) = h^j h^k (e^{1/f^*} - 1) \tag{4.1}$$

where f^* is the M-frequency and h^j is the offset. Thus the instantaneous frequency, f, at time h^k associated with the M-frequency f^* is

$$f(h^k; f^*) = [h^j h^k (e^{1/f^*} - 1)]^{-1}. \tag{4.2}$$

It should be noted that the M-period and M-frequency are constant for an M-periodic function, but the instantaneous period increases linearly over time while the instantaneous frequency decreases. If $g(t)$ is an M-periodic function then $\delta = h^m$ is the M-period of $g(t)$, where $h > 1$ and m is the smallest positive integer such

that $g(h^k) = g(h^{k+m})$ for all $h^k \in I$. Since $f^* = (\ln \delta)^{-1} = 1/(m \ln h)$, it follows that $\delta = h^m = e^{1/f^*}$. Thus the instantaneous period at h^k of an M-periodic function is $l_k = h^{k+m} - h^k = h^k(e^{1/f^*} - 1)$, while the instantaneous frequency is the reciprocal of l_k, i.e., l_k^{-1}. These comments motivated the definitions in (4.1) and (4.2) above. As we have seen from (2.10), the M-autocorrelation of an Euler process is a linear combination of terms that possess the following properties among others:

(i) If the associated root of the characteristic equation is complex and on the unit circle, the corresponding term in the M-autocorrelation is M-periodic.
(ii) If the root is complex and outside the unit circle, this term is a damped M-periodic function.

It follows then that any root of the characteristic equation that is complex and close to the unit circle will contribute a linearly elongating cyclic behavior to the data.

4.1. *Instantaneous Spectrum*

From (4.2) it follows, for any fixed h^j, that the instantaneous frequency $f = f(h^k; f^*)$ depends on time t, h^k, and f^*. Moreover, from (4.2) it follows that if $t = h^k$,

$$f^* = \left[\ln \left(\frac{1 + fh^j h^k}{fh^j h^k} \right) \right]^{-1}. \tag{4.3}$$

This leads to the following definition.

Definition 4.2. The instantaneous spectrum of $X(t)$ at $t = h^k$ is defined by

$$S(f, h^k; h^j) = G_X(f^*). \tag{4.4}$$

Definition 4.3. If $X(t)$ is a continuous M-stationary process, the instantaneous spectrum of $X(t)$, $t \in (-\infty, \infty)$ is defined by

$$S(f, t; t_0) = \Sigma_X(f^*)$$

where $t \in (-\infty, \infty)$ and t_0 is the origin offset (or realization offset).

It should be noted that at each time h^k and fixed h^j, the instantaneous frequency is in cycles/sampling unit based on the sampling units of the equally spaced data set.

5. Forecasting from an Euler(p) Model When Data are Observed at Euler Time Points

Even though data will usually be taken at equally spaced time points, in this section we consider the case in which data are observed at points $t = h^{j+k}$ for a specified j, and $k = 1, 2, \ldots, n$. We will say that such data are observed at Euler time points. Because of the dual relationship between discrete Euler(p) and discrete AR(p) processes, the parameter estimation method for discrete Euler(p) processes is strongly related to that of discrete AR(p) processes. That is, when we estimate the parameters of the dual discrete AR(p) process, we obtain the parameter estimates of the corresponding

Euler(p) process. However, in this section we will obtain forecasts for data observed at Euler time points from a known Euler(p) model where h and h^j are also known.

For a discrete AR(p) process, it is well known that the l-step ahead forecast function given data to t_0 is the solution of the corresponding pth order difference equation that passes through the last p points. In other words, if we denote the l-step ahead forecast by $\widehat{Y}_{t_0}(l)$, then

$$\widehat{Y}_{t_0}(l) - \phi_1\widehat{Y}_{t_0}(l-1) - \phi_2\widehat{Y}_{t_0}(l-2) - \cdots - \phi_p\widehat{Y}_{t_0}(l-p) = 0\,. \tag{5.1}$$

Letting $T_0 = h^{t_0}$, we then denote the l-step ahead forecast for $X(h^{t_0+l})$ given data to T_0 by $\widehat{X}_{T_0}(h^l) = \widehat{X}(h^{t_0+l}) = \widehat{X}(T_0h^l)$. Note also that since $Y_k = X(h^k)$, we define forecasts using the relationship $\widehat{X}_{T_0}(h^l) = \widehat{Y}_{t_0}(l)$ where $\widehat{Y}_{t_0}(l)$ is the usual l-step ahead forecast of a stationary AR(p) process.

If Y_t is the AR(1) process $Y_t - \phi_1 Y_{t-1} = a_t$, then it is well known that $\widehat{Y}_{t_0}(l) = Y_{t_0}\phi_1^l$. Thus, it follows that if $X(h^k)$ is a first-order discrete Euler process, then

$$\widehat{X}_{T_0}(h^l) = Y_{t_0}\phi_1^l = \widehat{X}_{T_0}(1)\phi_1^l = \widehat{X}_{T_0}(1)\alpha^{\ln h^l} \tag{5.2}$$

where $\alpha = \phi_1^{1/\ln h}$. If $X(h^k)$ is a second-order discrete Euler process with dual process $Y_k - \phi_1 Y_{k-1} - \phi_2 Y_{k-2} = a_k$, then based on standard results for forecasts from AR(2) processes (see e.g., Box et al., 1994), if the roots of the characteristic equation $1 - \phi_1 r - \phi_2 r^2 = 0$ are both positive and distinct, it follows that

$$\widehat{X}_{T_0}(h^l) = \widehat{Y}_{t_0}(l) = c_1 r_1^{-l} + c_2 r_2^{-l} = c_1\alpha_1^{-\ln h^l} + c_2\alpha_2^{-\ln h^l}$$

where c_1 and c_2 are real constants determined by $x(h^{t_0})$ and $x(h^{t_0-1})$ and where $\alpha_1 = r_1^{1/\ln h}$ and $\alpha_2 = r_2^{1/\ln h}$. Furthermore, if the roots of the characteristic equation are complex, i.e., $r = a \pm bi$, then it follows that

$$\begin{aligned}\widehat{X}_{T_0}(h^l) = \widehat{Y}_{t_0}(l) &= |R|^{-l}\{c_1\cos vl + c_2\sin vl\}\\ &= |R_h|^{-\ln h^l}\{c_1\cos\beta\,\ln h^l + c_2\sin\beta\,\ln h^l\}\end{aligned}$$

where $R = \sqrt{a^2+b^2}$, $v = \tan^{-1}(b/a)$, $R_h = R^{1/\ln h}$, and $\beta = v/\ln h$. Again, c_1 and c_2 are real constants determined by $x(h^{t_0})$ and $x(h^{t_0-1})$.

All the above results are useful in understanding the nature of forecasting on the log scale. However, the actual computation of a forecast will be based on the relationship

$$\widehat{X}_{T_0}(h^l) - \phi_1\widehat{X}_{T_0}(h^{l-1}) - \cdots - \phi_p\widehat{X}_{T_0}(h^{l-p}) = 0$$

for $l \geq 1$. Thus, forecasts can be obtained recursively as

$$\begin{aligned}\widehat{X}_{T_0}(h) &= \phi_1 X(h^{t_0}) + \cdots + \phi_p X(h^{t_0-p+1}),\\ \widehat{X}_{T_0}(h^2) &= \phi_1\widehat{X}_{T_0}(h) + \phi_2 X(h^{t_0})\cdots + \phi_p X(h^{t_0-p+2}),\end{aligned}$$

and similarly for $\widehat{X}_{T_0}(h^l)$, $l > 2$.

6. Data Observed at Equally Spaced Time Points

A data set observed at equally spaced time intervals must be treated differently from a data set observed at Euler time points even though both are taken from the same underlying M-stationary process (see Vijverberg, 2002; Vijverberg and Gray, 2003). Since most real data are equally spaced it is important to have procedures for estimating the parameters of the underlying Euler(p) model and subsequently obtaining forecasts when the observed data are equally spaced.

Suppose we are given data $X(1+\alpha), X(2+\alpha), \ldots, X(n+\alpha)$, where $\alpha \geq 0$, which we consider to be data from a continuous Euler process, where n is the number of observed values and α is an unknown shift of the sample from the process origin. In this section we describe a procedure for estimating the parameters of the Euler(p) model, including h and α. Additionally, for a given model and equally spaced data $X(1+\alpha)$, $X(2+\alpha), \ldots, X(T+\alpha)$ up to the forecast origin $T+\alpha$, we describe a technique for forecasting $X(T+\alpha+m)$, where $m \geq 1$ is an integer.

The procedure for estimating the underlying Euler(p) model and its parameters is described below. See Vijverberg and Gray (2003) for further discussion of this procedure. Before specifying the steps, it should be noted that h and α are selected together as a pair. Specifically, for a given α we select h so that the number of data points in the dual will be the same number (n) as there are in the original data set. Thus, for a given α, the values for j and h are determined by letting j be the largest integer such that $h^{j+1} \geq \alpha+1$ and $h^j < \alpha+1$, i.e., $j = (\ln(\alpha+1)/\ln h) - \delta$ where δ is the fractional part of $\ln(\alpha+1)/\ln h$. Also, the last Euler time point should be equal to the last equally spaced time point, i.e., $h^{j+n} = \alpha+n$. Substituting $j = (\ln(\alpha+1)/\ln h) - \delta$ into this equality, we obtain $h = \left(\frac{\alpha+n}{\alpha+1}\right)^{1/(n-\delta)}$. Since $0 < \delta < 1$ depends on h, in practice we approximate h using $h = \left(\frac{\alpha+n}{\alpha+1}\right)^{1/(n-.5)}$. Based on the given data and the resulting h and j, we interpolate the data at the Euler time points, i.e., $t = h^{j+k}$, $k = 1, \ldots, n$. Note that h^j is the origin offset or realization offset defined earlier. Several methods are available for interpolation, and it should be noted that in the examples discussed here we use standard linear interpolation.

The current procedure (which is still evolving) is as follows:

1. For each α in a predetermined range of possible values:
   (a) We obtain the corresponding h and the interpolated data at the Euler time points $t = h^{j+k}$, $k = 1, \ldots, n$.
   (b) The values at the Euler time points correspond to a dual AR(p) process for which we can use traditional methods for identifying p and obtaining the resulting coefficient estimates. The estimated model then corresponds to an Euler model.
   (c) From the estimated model obtained in (b) we can obtain estimated data values at $t = h^{j+k}$, $k = 1, \ldots, n$. Using these modeled values at the Euler time points, we interpolate to obtain model-based values at the original equally spaced time points with the specified α. A weighted sum-of-squared residuals (or, alternatively, the AIC) between the actual dual process and the model-based values of the dual is then calculated.
2. Steps (a)–(c) above are repeated for each α ranging over the predetermined range of possible values. The values of h and j resulting from the value of α with the minimum weighted sum-of-squared residuals (or the minimum AIC if desired) are selected as the estimates of h and j.

The procedure outlined in Steps 1–2 above produces an estimated model for the observed equally spaced data. In the following we describe a technique for obtaining forecasts based on a given model and equally spaced data $X(1+\alpha)$, $X(2+\alpha), \ldots, X(T_0+\alpha)$ where $T_0+\alpha$ is the forecast origin. We wish to find a forecast function for $X(T_0+\alpha+k), k=1,\ldots,m$. In order to obtain $\widehat{X}(T_0+\alpha+k)$ we proceed as follows.

3. Based on the estimated values of h and j, we can interpolate Euler data as in the above and estimate the parameters of the associated Euler model. The forecasts can be obtained as described in Sec. 5. We can, therefore, find the forecasts at $t = h^{j+T_0+q}, q=1,2,\ldots,m_1$, where m_1 is determined as follows: Letting $h^{j+n+m_1'} = \alpha+T_0+m$ we have $m_1' \approx \frac{\ln(\alpha+T_0+m)}{\ln h} - (j+n)$. Then, $m_1 = [m_1'+1]$ where $[\gamma]$ denotes the greatest integer that does not exceed γ.
4. The forecasts $\widehat{X}(h^{j+T_0+1}), \widehat{X}(h^{j+T_0+2}), \ldots, \widehat{X}(h^{j+T_0+m_1})$ are then used to interpolate to obtain forecasts at the desired time points, i.e., $\widehat{X}(T_0+\alpha+1), \widehat{X}(T_0+\alpha+2), \ldots, \widehat{X}(T_0+\alpha+m)$.

It should be pointed out that Steps 1–2 above provide an Euler model fit to the data. After this is obtained, not only can forecasts be obtained as mentioned above, but also the estimated model and associated data at Euler time points can be used to provide spectral estimates.

Remark. Software for modeling M-stationary processes as well as for forecasting and spectral estimation is available and can be downloaded from the authors' website. Specific instructions as well as a user's manual are included there.

7. Examples

Example 7.1. We refer again to the realization in Fig. 1 of equally spaced data values generated from the discrete Euler(2) model in (3.1) where $h=1.01$, $\alpha = h^j = 20$, $n=200$, and $\sigma_Z^2 = 1$. To illustrate the difference between the AR and Euler forecasts, we assume that we are only given the first 170 equally spaced observed data, and we want to forecast the next 30 data points. Thus, we have $n=170$ and $m=30$ in this case. The dual process is the AR(2) model $Y_k - 1.732Y_{k-1} + .98Y_{k-2} = z_k$. We follow the procedures mentioned above to estimate the offset. Using $(0,60)$ as the predetermined range of allowable values of h^j and allowing AIC to select up to an Euler (10) model, the procedure discussed in the previous section selects an Euler(3) model with $\hat{h} = 1.0118$ and $\hat{h}^j = 26$. By using the estimated offset, we interpolate values at Euler time points and estimate the parameters of the Euler model. The estimated parameters are $\hat{\phi}_1 = 1.452$, $\hat{\phi}_2 = -.764$, and $\hat{\phi}_3 = -.125$. The factors of this third-order model are displayed in Table 1. This presentation breaks

Table 1
Factor table for Euler(3) fit for data in Example 1, $\hat{h} = 1.0118$

Absolute reciprocal	M-frequency	Dual frequency	Factors
.984	8.7	.102	$1 - 1.581B + .968B^2$
.129	42.6	.5	$1 + .129B$

a pth order autoregressive operator $1 - \phi_1 B - \cdots - \phi_p B^p$ into its irreducible first- and second-order factors. For an irreducible second-order factor of the form $1 - \alpha_1 B - \alpha_2 B^2$, the associated roots of $1 - \alpha_1 r - \alpha_2 r^2 = 0$ are complex, and the absolute reciprocal of these roots is $\sqrt{-\alpha_2}$. Additionally, an irreducible second-order factor is associated with a system frequency of $f = \frac{1}{2\pi}\cos^{-1}\left(\frac{\alpha_1}{2\sqrt{-\alpha_2}}\right)$. In this setting, the system frequency indicates the frequencies in the dual process and is referred to in the table as the "dual" frequency. Roots for which the absolute reciprocal is close to unity are close to the nonstationary region and are thus more dominant. For a first-order factor, $1 - \alpha_1 B$, the absolute reciprocal of the associated root is $|\alpha_1|$, and the system frequency is $f = 0$ if $\alpha_1 > 0$ and $f = .5$ if $\alpha_1 < 0$. In the table we show the dual frequency and the M-frequency, f^*, which is given by $f^* = f/\ln h$.The dual frequency corresponding to the second order $1 - 1.581B + .968B^2$ is .102. Since $\hat{h} = 1.0118$, the associated M-frequency is given by $.102/\ln(1.0118) = 8.7$ which is a reasonable estimate of the true M-frequency, i.e., $.08/\ln(1.01) = 8.04$. In Fig. 2 we show the l-step ahead forecasts (denoted by "+") from the fitted Euler(3) model. Additionally, we analyzed the original data set as an AR(p) model. In this case, AIC picked an AR(10). In Fig. 2 we show the l-step ahead forecasts (denoted by a dashed line) from the fitted AR(10) model, and it is visually apparent that the Euler(3) forecasts are much better than the AR(10) forecasts as of course is expected. More specifically, the mean square forecast errors of the last 30 points is 7.2 for the Euler(3) model and 142 for the AR(10). The Euler(3) model appropriately interprets the expanding periodic behavior of the data. On the other hand, the AR-based analysis considers the data to be a realization of a stationary process with fixed frequencies. Thus, the periodic behavior seen in the forecasts is essentially an averaging of the periodic components for the entire realization and fails to adjust for the fact that the cycles are lengthening. Probably more important are the results shown in Fig. 3 where we show the spectral estimates associated with the Euler(3) fit. In Fig. 3(a) it can be seen that the M-spectrum has a single sharp peak.

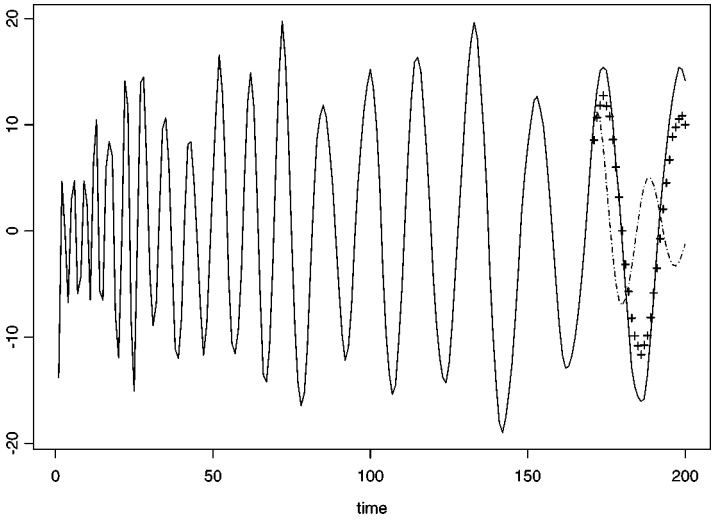

Figure 2. AR forecasts (dashed line), and Euler forecasts ("+") with $h = 1.0118$ and $\hat{\lambda} = 26$ based on the realization in Fig. 1.

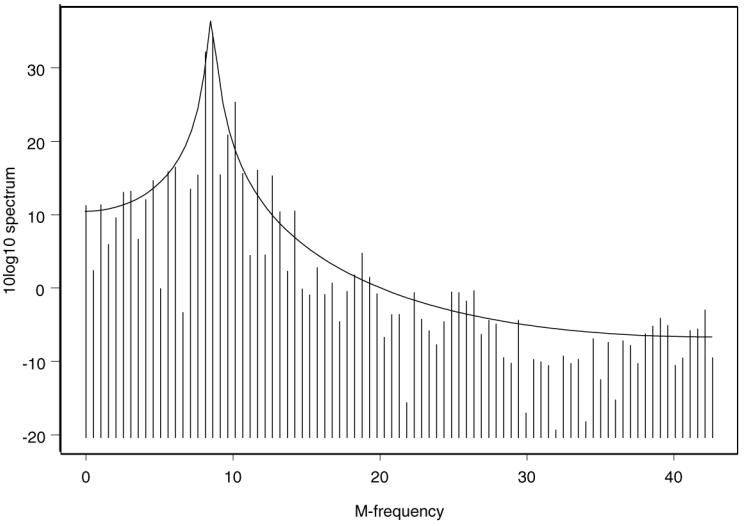

(a) M-Spectrum

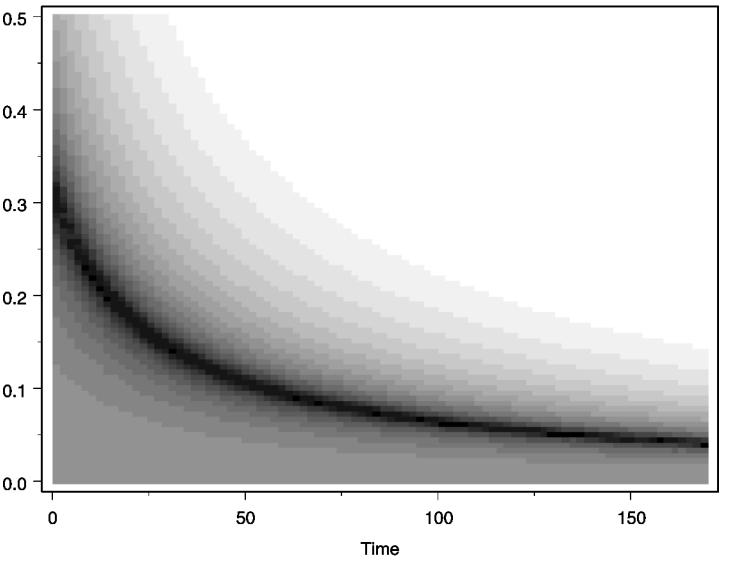

(b) Instantaneous Spectrum

Figure 3. Spectral plots based on Euler(3) fit to realization in Fig. 1.

In the instantaneous spectrum in Figure 3(b) it can be seen that the instantaneous frequency at the beginning of the series is at about $f = .3$, while at the end of the realization the instantaneous frequency has decreased to about .04. That is, initially, cycle lengths are about 3 while at the end of the series there are approximately 25 points per cycles. Examination of Fig. 1 will show that this is indeed the case.

7.1. *Analysis of Bat Echolocation Data*

The problem of identifying bats by their echolocation signal is one of great interest to many scientists, and several methods for characterizing such signals have been employed. Such methods include standard spectral analysis, wavelet analysis, window methods, and decision tree classification methods as well as others. To date, such approaches have met with varying degrees of success. For example, in Herr et al. (1997), 95% of the bats in 4 of 8 species were correctly classified, but in the remaining 4 species, 2 of the species were misclassified in 100% of the trials and the remaining 2 species were misclassified 96 and 51% of the time. According to Herr et al. (1997), "A new approach is required which considers other characteristics of the calls in more detail, such as shape of the pulses (frequency change over time) in each call." To support their conclusions, via sonograms they showed that many of the echolocation signals possessed an instantaneous frequency behavior that could be well modeled over much of its range as $1/(at + b)$. Therefore, the instantaneous period is a linear function of time, and consequently the results of this article suggest that the Euler process should serve as a very good model for this type of data. In these last two examples, we will demonstrate that this is indeed the case. In fact, we will demonstrate that these data have a very well-defined M-frequency structure and an instantaneous spectrum that is totally hidden from standard measures based on stationary models.

Example 7.2. In this example, we consider echolocation data from a large brown bat. The data were obtained courtesy of Al Feng of the Beckman Center at the University of Illinois. The entire data set is shown in Fig. 4(a) while close-ups of the first 100 and the last 60 points are shown in Fig. 4(b). The data consist of 381 data points taken at 7-microsecond intervals with a total duration of .0026671 seconds. Unlike our previous examples, the instantaneous period does not appear to be linear over the entire signal. In fact, the signal appears to be made up of possibly two different signals. However, we will consider the application of the Euler model to this data set and compare its usefulness with the autoregressive model. Based on the AIC, an AR(20) was fit to the data using standard methods, and using the methodology described here, an Euler(11) with offset equal to 203 was determined to be the best Euler model. In each case a maximum model of order 20 was considered. Tables 2 and 3 show the factors of the AR(20) and Euler(11) models along with the corresponding frequencies and their proximity to the unit circle. Figures 5(a) and 5(b) show the sample ACF and the sample M-ACF, respectively. Figure 6(a) shows the sample spectrum and the AR(20) spectral estimator, while Fig. 6(b) shows the M-sample spectrum and the Euler(11) spectral estimator. The lack of an indication of a periodic component in the sample ACF, sample spectrum, and AR(20) spectral estimator are quite surprising in view of the cyclic appearance of the data. This is due to the fact that although there certainly is a cyclic nature to the data, the cycle is lengthening slightly with time. As a result, the usual spectrum is spread and the correlation changes with time resulting in the sample estimates shown in Figs. 5(a) and 6(a). It should be pointed out that even though the Euler process has an elongating period, the M-ACF does not depend on time, nor does the M-spectrum. Figures 5(b) and 6(b) clearly indicate the cyclic behavior of the data on the log scale. It is important to note that the energy in the signal is primarily concentrated at approximately the M-frequencies $53k, k = 0, 1, 2, 3$. We will refer to the case $k = 1$ as M-fundamental frequency and $k = 2, 3$ as M-harmonics.

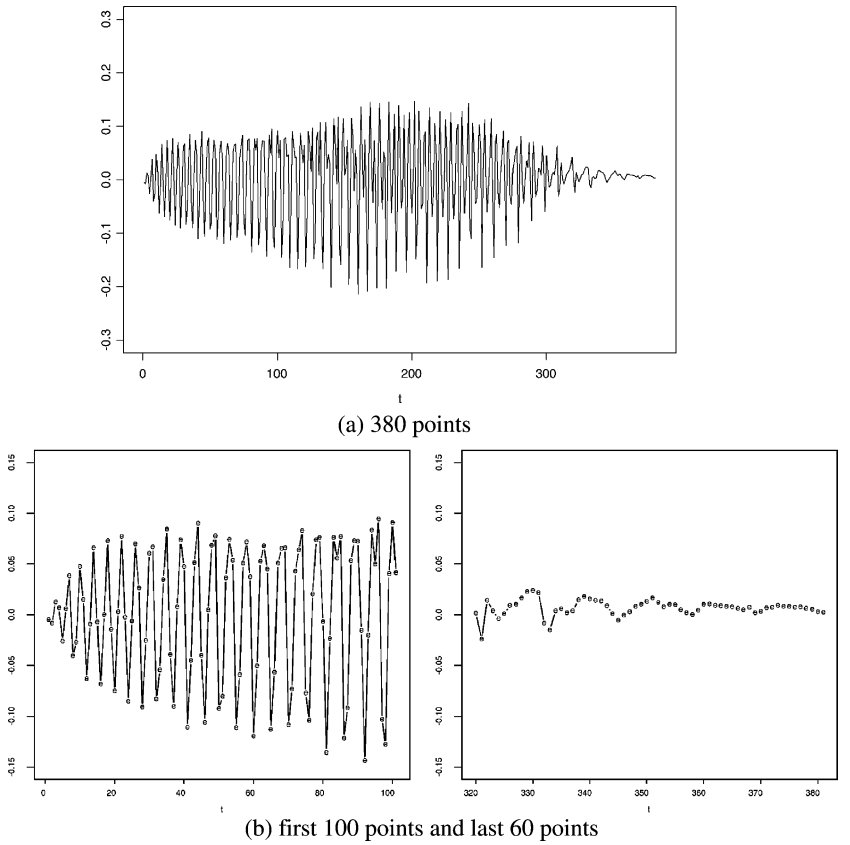

Figure 4. Plot of echolocation data for large brown bat.

Figures 7(a) and 7(b) show the residuals of the AR(20) fit and the Euler(11) model. Even though some correlation still remains in the residuals, most of the variation in the data has been accounted for in the case of the Euler(11). Higher orders do not improve the fit.

Although it is not our primary interest, forecasting from different origins provides insight into the fit of the two models. Figure 8(a) compares the AR forecast with the Euler forecasts from points 40 to 80, while Fig. 8(b) compares the forecasts for the last 24 points. It is obvious in both cases that the AR forecasts quickly become out of phase while the Euler forecasts track the signal well. Thus the Euler model seems to provide a good fit for these data.

Earlier we introduced the instantaneous spectrum that displays the variance (or power) in the signal at each instantaneous frequency and time. Let the time series be recorded at the integers of a time scale denoted by t, i.e., on this scale, the observed values occur at equally spaced times $t = 1, \ldots, n$. Since the origin offset was estimated to be $\hat{\alpha} = 203$, then the sampled values are actually at time points $t_\alpha = \hat{\alpha} + t = 203 + t$. Thus, the M-frequency is mapped into an instantaneous frequency at each t. Instantaneous frequency is frequency in the usual sense, i.e., cycles per sampling unit. Figure 9 shows the instantaneous spectrum $\widehat{S}(f, h^k; h^j)$ for $0 \leq f \leq .5$ and $t_\alpha \in (203, 584)$ associated with the Euler(11). The graph uses a gray

Table 2
Factor table for AR(20) fit for large brown bat data

Absolute reciprocal	Frequency	Factors
.997	.0	$1 - .997B$
.960	.149	$1 - 1.141B + .922B^2$
.950	.097	$1 - 1.557B + .903B^2$
.930	.178	$1 - .817B + .864B^2$
.919	.500	$1 + .919B$
.905	.258	$1 + .094B + .819B^2$
.892	.225	$1 - .274B + .795B^2$
.890	.299	$1 + .540B + .792B^2$
.887	.441	$1 + 1.652B + .787B^2$
.884	.389	$1 + 1.357B + .782B^2$
.878	.341	$1 + .952B + .771B^2$

scale to show the amplitude of the instantaneous spectrum, $\widehat{S}(f, h^k; h^j)$, at (f, t) where $t = 1, \ldots, 381$. In this scale, dark regions represent larger spectral values. It should be noted that the instantaneous frequencies appear to be decreasing, indicating that the periods are lengthening. Thus, at the beginning of the data the major source of the variation is at frequencies .26 and above while at the end of the data the variation is concentrated at frequencies .27 and below. In this regard it is interesting to note that the instantaneous frequency, .26, associated with $f^* = 53$ at the initial observation, is almost exactly equal to the instantaneous frequency, .27, associated with $f^* = 157$ at the final data point $t = 381$ (i.e., $t_\alpha = 584$). Also it should be noted that the sampling rate is not quite fast enough at the beginning of the data. Again, since the origin offset is 203, then the actual times, t_α, at which observations are recorded are $204, 205, \ldots, 584$. The Nyquist frequency for the equally spaced data is $1/2$, so the highest instantaneous frequency that can be detected at a given t, is $f = f(h^k; f^*) \leq 1/2$. The instantaneous frequency at $t_\alpha = 212$, i.e., at $t = 9$, is given by $f(t; f^*) = [(\hat{\alpha} + t)(e^{1/f^*} - 1)]^{-1}$ which for $f^* = 106$ and $\hat{\alpha} = 212$ is given by $f(9; 106) = [212(e^{1/106} - 1)]^{-1} \approx .5$. Thus, beginning at about the 9th data value, we can detect the M-frequency $f^* = 106$. This is visually displayed in Fig. 9 in the sense that initially we cannot visually detect the frequencies associated with M-frequencies of 106 and 157. However, by the 9th data point we begin to

Table 3
Factor table for Euler(11) fit for large brown bat data, $\hat{h} = 1.00278$

Absolute reciprocal	M-frequency	Dual frequency	Factors
.997	53.2	.148	$1 - 1.195B + .993B^2$
.996	105.8	.294	$1 + .539B + .991B^2$
.970	0.0	.0	$1 - .97B$
.955	156.7	.435	$1 + 1.753B + .911B^2$
.706	61.1	.170	$1 - .684B + .498B^2$
.658	135.9	.377	$1 + .944B + .433B^2$

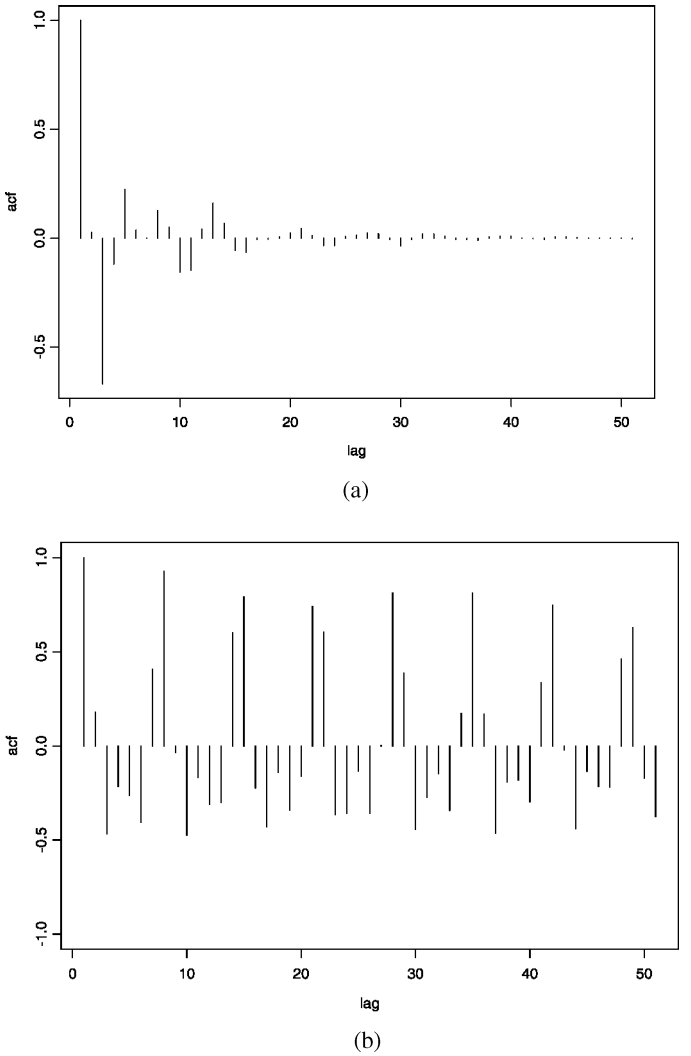

Figure 5. Sample ACF (a) and sample M-ACF for data in Fig. 6(a).

see the appearance of $f^* = 106$. Actually, we can detect M-frequencies up to 102 from the beginning. Although the power does fall off quickly in a neighborhood of 106, there is still significant power at 102. Consequently, the frequency at 106 can also essentially be seen from the beginning. However, the instantaneous frequency associated with $f^* = 157$ cannot be fully detected until about $t_\alpha = 314$, i.e., it cannot be fully seen until approximately the 111th observation in Fig. 4(a).

This now explains the unusual appearance of the data beginning around the 81st data point. It actually appears that the data are joined by an "interfering" signal at this point. However, this is not the case. Instead, up to this point, this highest frequency of the underlying signal has been too high to detect at this sample rate, and as a result has been completely aliased until approximately the 81st value at which point the associated instantaneous period becomes sufficiently long that it can

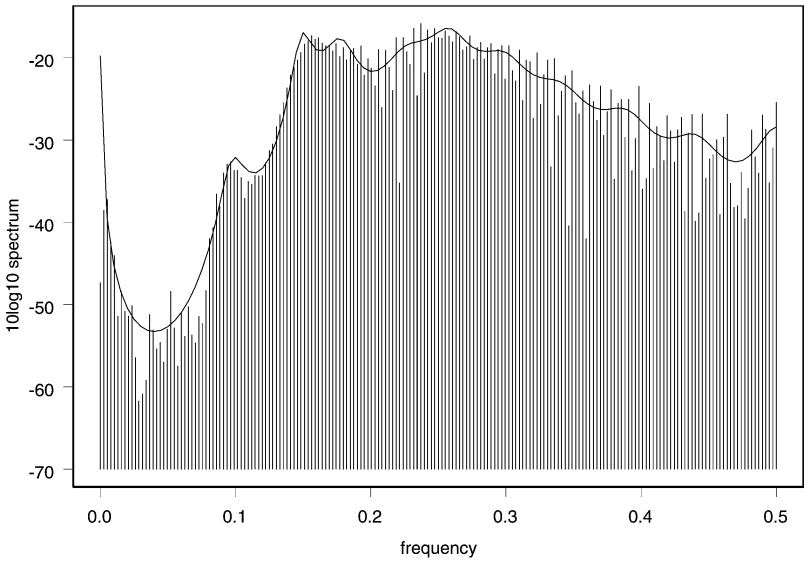

(a) Sample spectral density and AR(20) spectral density

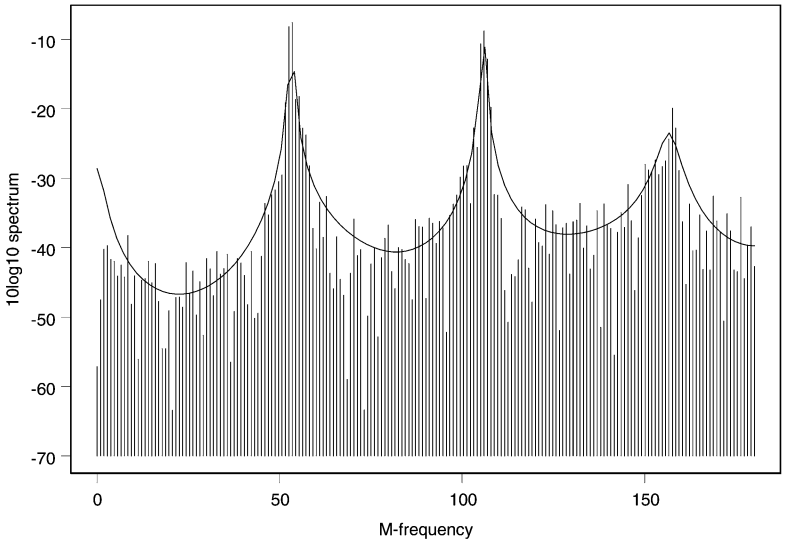

(a) Sample M-spectral density and Euler(11) spectral density

Figure 6. Spectral estimates for large brown bat data.

be seen. From the Euler(11) spectral estimator and the M-sample spectrum it can be seen that the power is increasing from about $f^* = 142$ to the peak at $f^* = 157$. The appearance of a third cycle at about the 81st sample point (i.e., before the 111th point) is due to the power in the signal in the neighborhood of the peak at $f^* = 157$.

In Fig. 10(a) we show the modulus of the continuous wavelet transform while in Fig. 10(b) we show the Gabor transform. These graphs were obtained using the

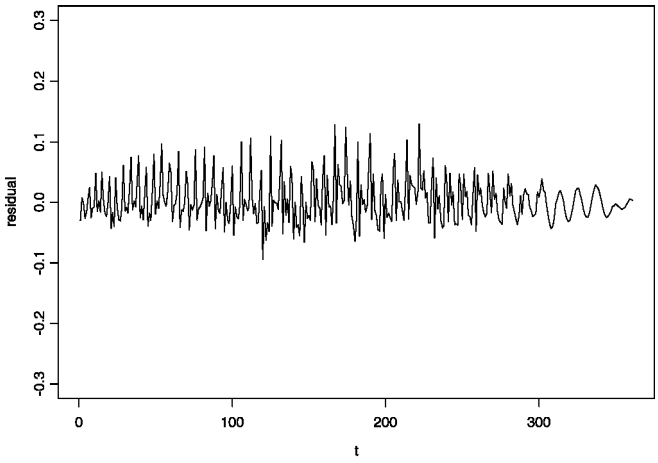

(a) Residuals from AR(20) fit

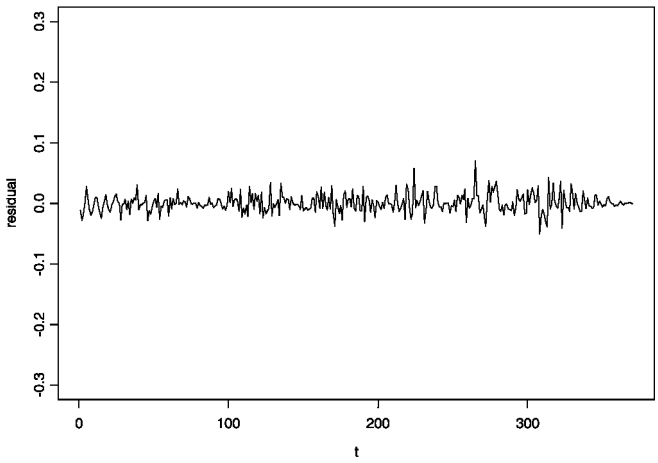

(b) Residuals from Euler(11) fit

Figure 7. Residuals from models fit to large brown bat data.

Rwave package, and involve a transformed version of the frequency axis. In the case of the wavelet transform the vertical axis is based on "scale" which is an inverted version of frequency. These window-based presentations of the time-varying spectral content also tend to show a portion of the fundamental and its first harmonic, and in the case of the Gabor transform, a slight indication of the second harmonic. However, the zero frequency is not visible in either case. Some improvement can be obtained by determining an optimal kernel based on the Wigner distribution. However, in these representations, the periodic behavior toward the beginning and end of the realization are not seen, and the second harmonic is barely visible while the zero frequency does not show up at all. (See http://www-dsp.rice.edu/software/optkernel.shtml.) As described above, examination of the data shows that the instantaneous spectrum does an excellent job of describing the

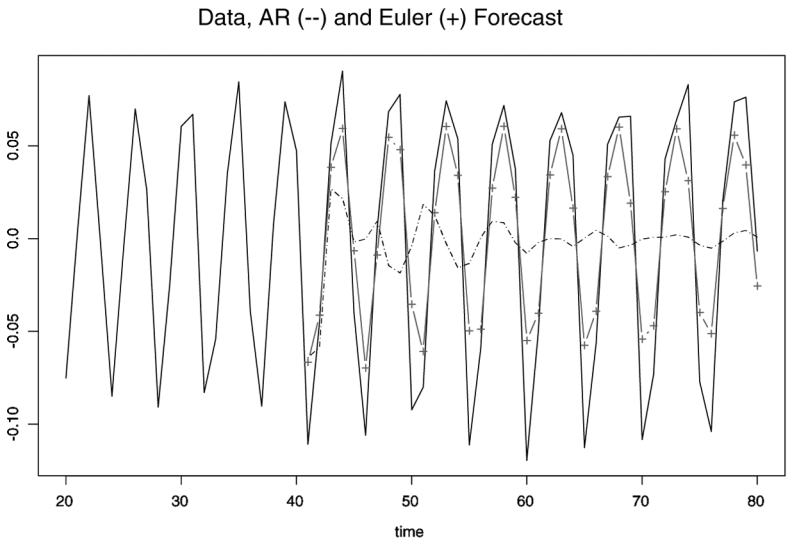

(a) Forecasts of points 40-80

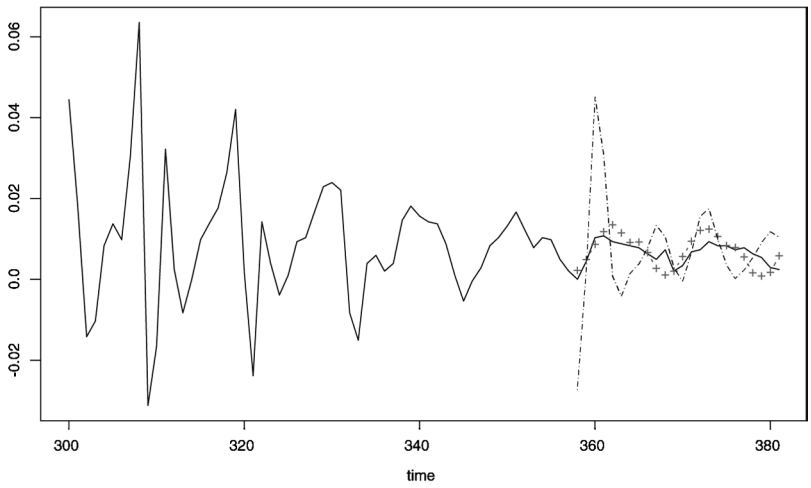

(b) Forecasts of the last 24 points

Figure 8. Forecasts based on AR(--) and Euler (++) fits to data in Fig. 4(a).

frequency behavior throughout the entire realization. The improvement is obtained since, in contrast to the window-based methods, M-stationary analysis actually uses the entire data set to estimate spectral information at each frequency. A remark should be made concerning the zero frequency. Since this frequency does not change with time, its graph essentially coincides with the t axis. As a result, the gray scale may not show the zero frequency as clearly as the other frequencies. However, inspection of the factor table or the M-spectrum confirms the presence of substantial power at the zero frequency.

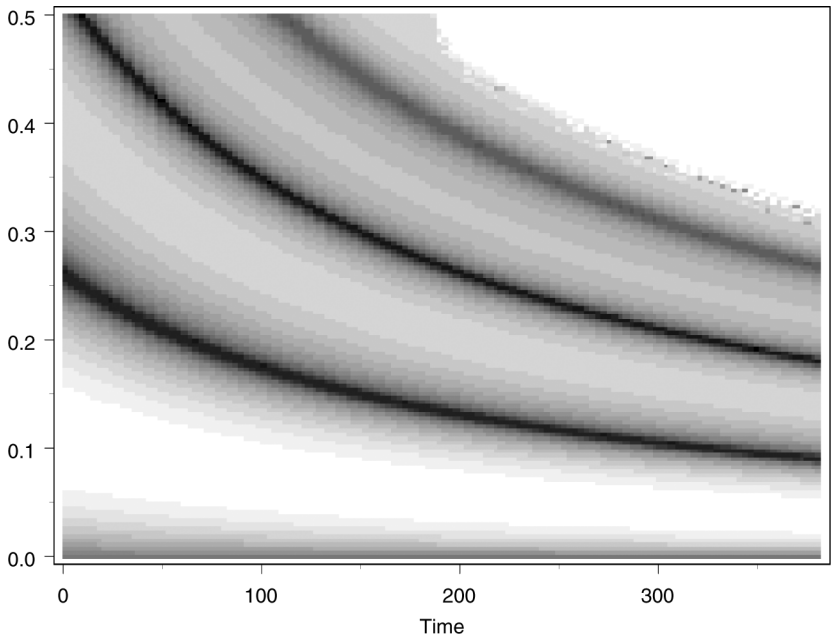

Figure 9. Instantaneous spectrum for Euler(11) fit to data in Fig. 4.

Another useful representation of the time-varying frequency behavior at time t can be obtained by plotting $S(f, t; A) = G_X(f^*)$ at the values of t where A is the origin offset. Thus, for each t one can obtain a spectral plot displaying the instantaneous frequency behavior in a format similar to the usual spectrum. For example, in Figs. 11(a)–(d) we show the time varying spectral plots for $t = 1, 14, 114,$ and 381. There it can be seen that at $t = 1$ only one peak is visible, while the second peak is seen by about the ninth observation. The third peak in the spectrum begins to appear by time $t = 114$, and at the end of the series, three peaks are still present. In general it is clear that M-frequencies are being mapped into instantaneous frequencies at time t are becoming closer to zero (i.e., are becoming lower frequency) as t increases.

To summarize, we note the following.

1. The M-stationary model seems to be an excellent model for the data and is far superior to the AR model in this case, even though the period is expanding slowly.
2. The notion of instantaneous frequency has been well demonstrated and it has shown that for a fixed h^j, $f = f(h^k; f*)$ so that the M-frequency determines the instantaneous frequency at each time point.
3. We have provided a useful visualization of the spectral content of the linearly expanding periodicity (and the corresponding decaying frequency) in time.
4. It was demonstrated that as time evolves and periods lengthen, frequencies not seen previously in the data may become visible as time increases.

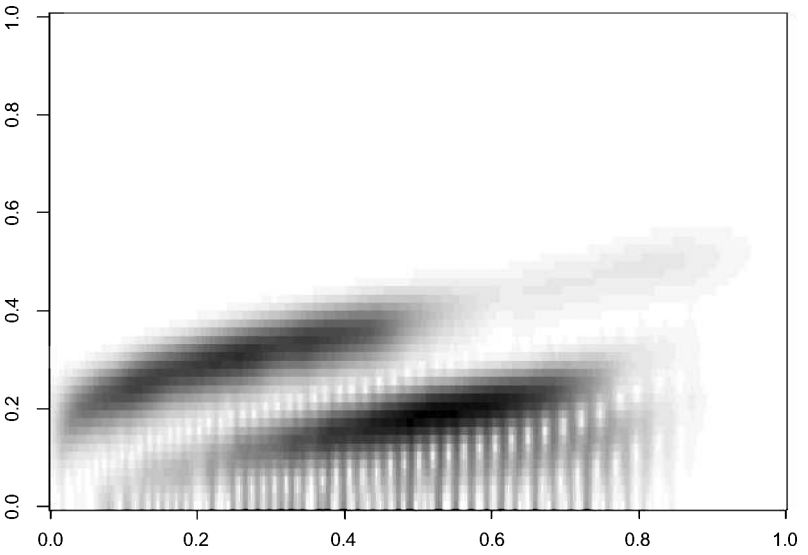

(a) Continuous wavelet transform using the Morlet wavelet

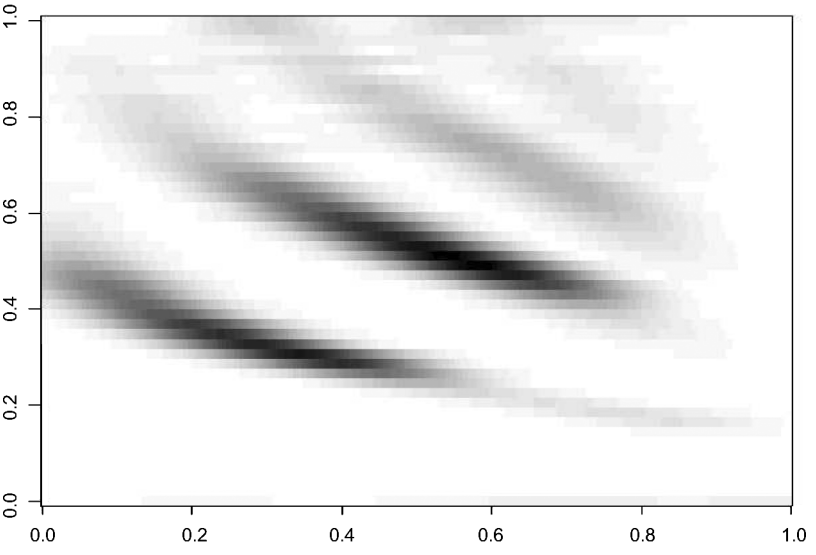

(b) Gabor transform

Figure 10. Window-based representations for data in Fig. 4(a).

In this example, from the start there was a question as to whether or not autoregressive or M-stationary models were appropriate. As it turned out, the AR model was not satisfactory and the M-stationary model performed very well.

In the next example we consider another bat signal where at a glance, it is not obvious that an AR model is not satisfactory. However, the software referenced

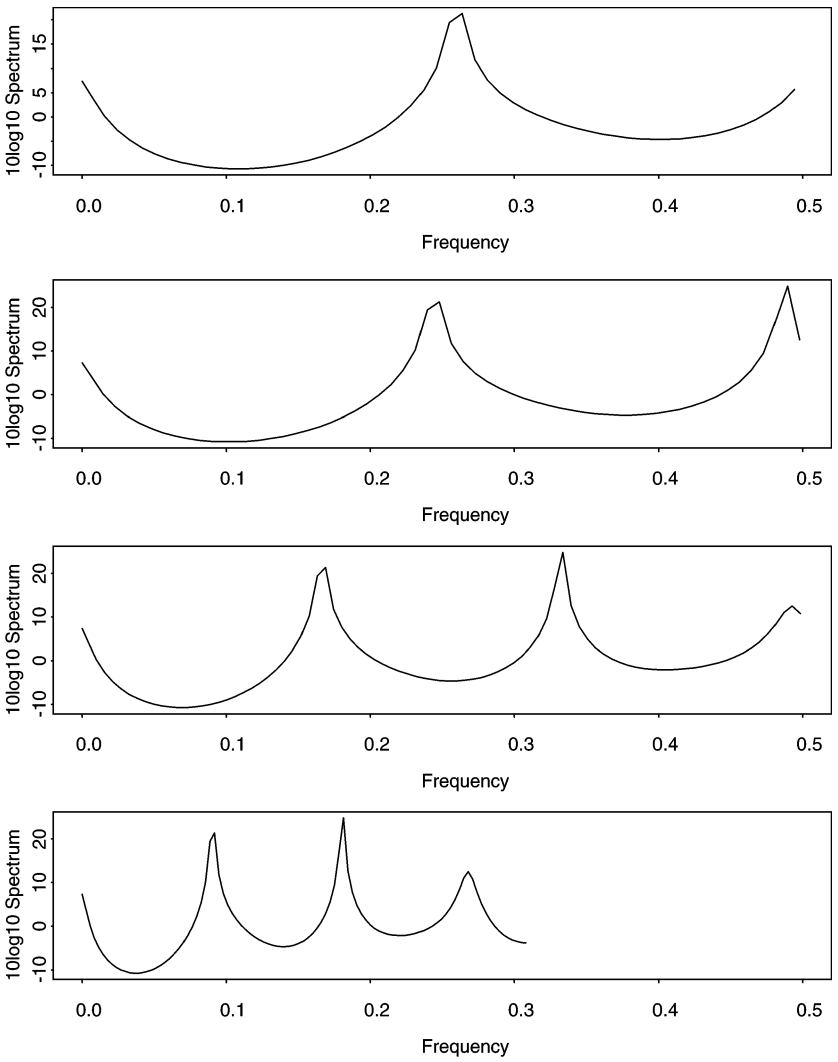

Figure 11. Spectral plots showing instantaneous frequency behavior in data from Fig. 4(a) at four different time points. Top left, $t = 1$; top right, $t = 14$; bottom left, $t = 115$; bottom right, $t = 381$.

earlier does identify the M-stationary model as the appropriate model. This will be explained in more detail in the final section of this article.

Example 7.3. The data consist of 280 observations taken from a Nyctalus noctula hunting bat echolocation signal at 4×10^{-5} second intervals. This data set was studied recently by Jiang et al. (2003). We briefly analyze these data in the same manner as the previous example and find a strong similarity in structure, although the frequencies involved are quite different. We compare the AR model to the Euler models for purposes of describing the behavior of the data. In this case AIC selects an AR(7) while the algorithm introduced here picks an Euler(12) with origin offset 188 where a maximum order of 13 was allowed in each case. Figure 12 shows the

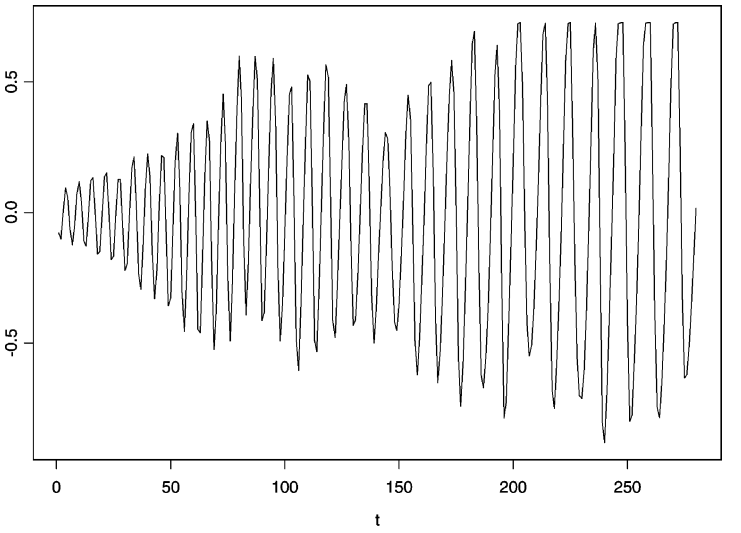

Figure 12. Echolocation signal from a Nyctalus noctula hunting bat.

data, and close inspection indicates that the cycles are indeed elongating. Figure 13 shows the forecasts of the last 30 points using the AR and Euler models. It can be seen that the Euler forecasts do an excellent job of tracking the elongating cyclic behavior while the AR forecasts quickly get out of phase.

Figure 14(a) shows the sample spectrum and the AR(7) spectral estimator while Fig. 14(b) shows the M-sample spectrum and the Euler(12) spectral estimator. Inspection of Fig. 14(a) shows that the AR model gives a very broad spectrum. However, Fig. 14(b) indicates that the Euler model has M-frequencies primarily

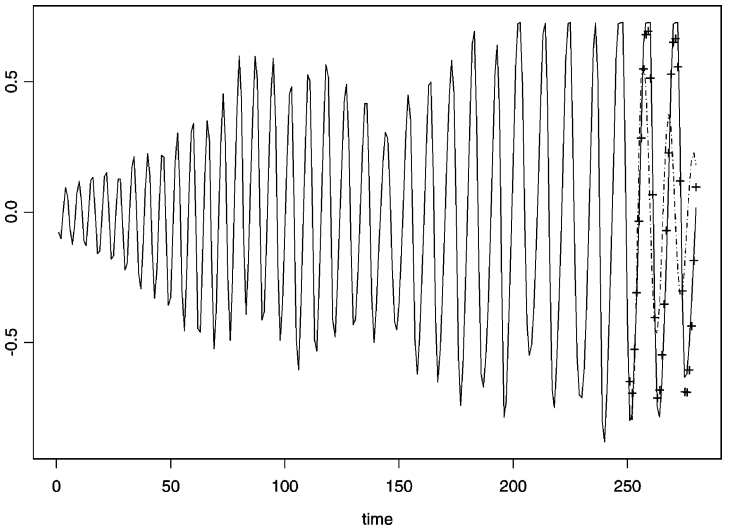

Figure 13. Forecasts of AR(–) and Euler(++): the last 30 points.

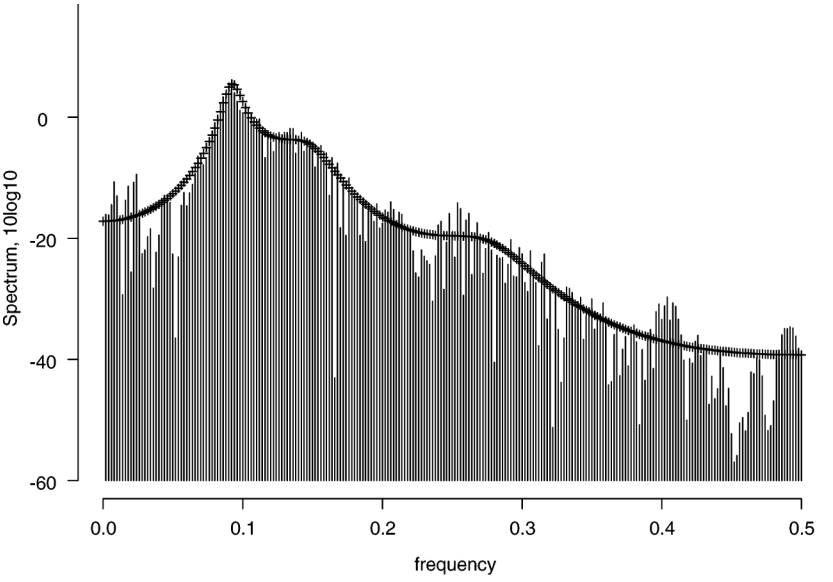

(a) Sample Spectrum and AR(7) Spectral Estimator

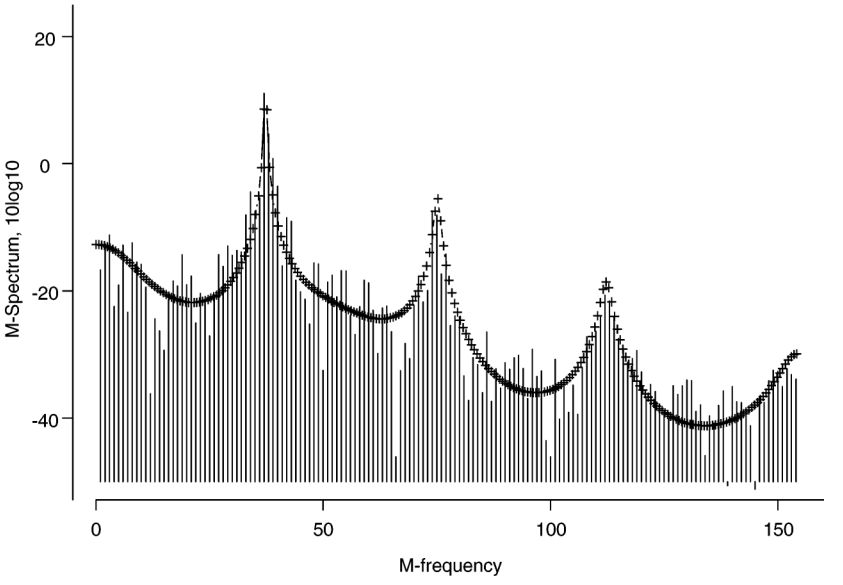

(b) Sample M-spectrum and Euler(12) Spectral Estimator

Figure 14. Spectral estimators for Nyctalus noctula hunting bat signal.

concentrated at the M-fundamental and its M-harmonics, which in this case are given by $37k$, $k = 1, 2, 3$ along with a peak at zero. These peaks are clearly seen in Fig. 14(b) and are also displayed in Table 4 where the factors of the Euler(12) model are shown along with their proximity to the unit circle. It is clear that the highest M-frequency that will have much effect on the cycles in the data is $f^* = 112$.

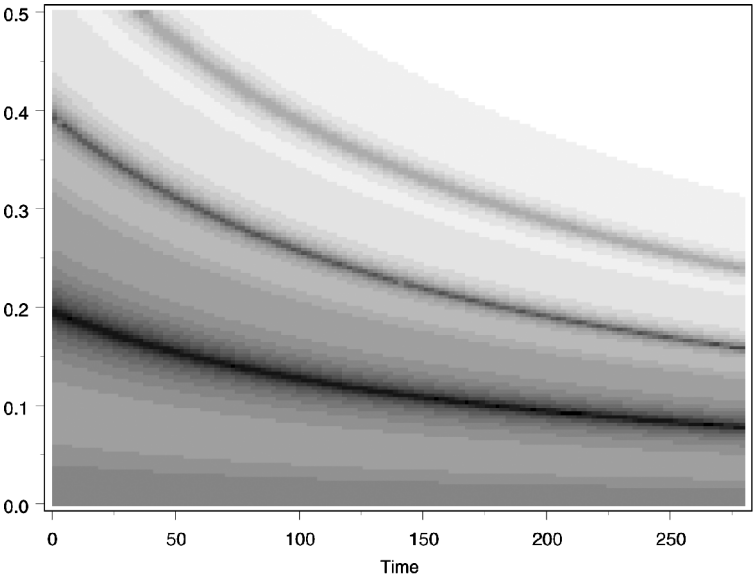

(a) Sample Instantaneous Spectrum

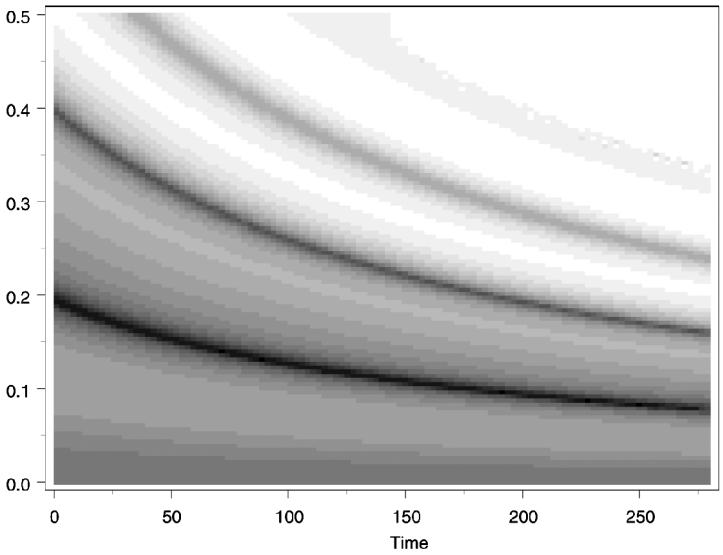

(b) Euler(12) Instantaneous Spectrum

Figure 15. Instantaneous spectral estimates for data in Fig. 11.

Figure 15(a) shows the sample instantaneous spectrum (i.e., the instantaneous spectrum based on the sample M-spectrum) while Fig. 15b shows the Euler(12) instantaneous spectrum. There the harmonics seen in Fig. 14(b) are clearly visible in both plots and it can be seen that the frequency behavior is decreasing with time. Also in both plots it can be seen that the instantaneous frequency, .20, associated with the M-fundamental frequency, i.e., $f^* = 37$, at the beginning of the data is

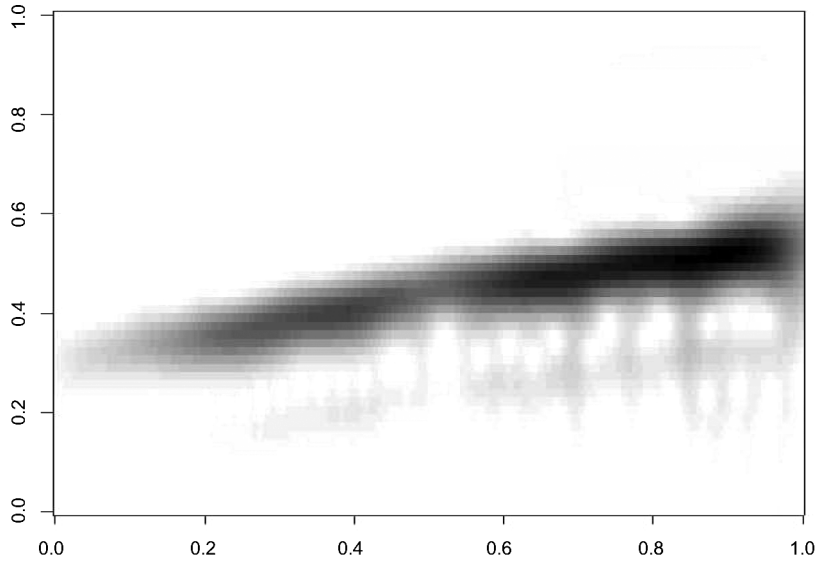

(a) Continuous wavelet transform using Morlet wavelet

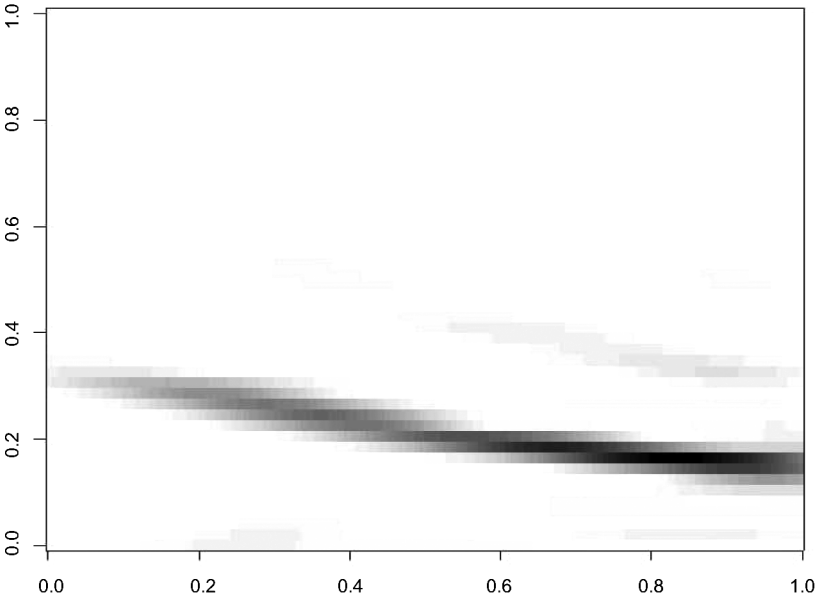

(b) Gabor transform

Figure 16. Window-based representations for data in Fig. 11.

higher than the instantaneous frequency, .16, associated with the M-frequency of the middle peak in the M-spectrum, i.e., $f^* = 75$, at the end of the data set. A similar behavior was noted in Example 7.2. In Fig. 16 we show the continuous wavelet and Gabor transforms of the hunting bat echolocation signal. Interestingly, these transforms only show one time-varying frequency in the data.

Table 4
Factor table for Euler(12) fit for nyctalus noctula hunting bat data, $h = 1.00326$

Absolute reciprocal	M-frequency	Dual frequency	Factors
.998	37	.12	$1 - 1.445B + .995B^2$
.986	75	.24	$1 - .070B + .972B^2$
.959	112	.37	$1 + 1.269B + .919B^2$
.872	6	.02	$1 - 1.728B + .760B^2$
.809	52	.17	$1 - .789B + .654B^2$
.759	147	.48	$1 + 1.502B + .576B^2$

Realizations of length $n = 280$ were generated from the Euler(12) model factored in Table 4 in order to compare the instantaneous spectrum with the Gabor and wavelet transforms. In Fig. 17(a) we show the instantaneous spectrum for a representative realization and in Fig. 17(b) we show the corresponding Gabor transform. From Table 4 and Fig. 13(b) it can be seen that the Euler (12) model used to generate the realization has multiple frequencies. It is clear that the instantaneous spectrum in Fig. 17(a) does a better job of identifying the multiple frequencies that are in the model than does the Gabor transform in Fig. 17(b). The wavelet transform gave results similar to those of the Gabor transform and is not shown here. The results shown in Fig. 17 are representative of those seen in the generated realizations.

Before concluding this example we note that transforming the frequency axis to Hz shows that the lowest frequency in Hz for the large brown bat in Example 7.2 ranges from 38,000 Hz at the beginning of the series to about 15,000 Hz at the end. These values are about an order of magnitude higher than those for the hunting bat.

7.2. *Monotonic Time Varying Frequencies (MTVF)*

As was stated earlier, the problem of the analysis of processes with time varying frequencies (TVF) is a long-standing one. Some of the more common data of this type are chirps and Doppler signals. For example, deterministic signals of the form $\cos[\beta_2 t^2 + \beta_1 t]$, $\cos[\beta_3 t^3 + \beta_2 t^2 + \beta_1 t]$ and $\cos[\theta_1 + \theta_2 e^{bt}]$, are referred to as linear, quadratic, and exponential chirps, respectively, and are quite common in radar, sonar, and communication theory. For an interesting medical application see Xu et al. (2000). All of these signals generally have monotonic time varying frequencies (MTVF) over the time period of interest.

An element of stochasticity can be added to each of these MTVF signals by adding random noise, and to date that is essentially the extent of progress in this area. However, using the time deformation method employed here it is possible to dramatically extend chirp, Doppler, and other MTVF signals to corresponding stochastic processes where, in essence, sets of such functions furnish the basis of the correlation structure in the same way as $\{\cos \beta_k t, \sin \beta_k t\}$ do for stationary models, and $\{\cos \beta_k \ln t, \sin \beta_k \ln t\}$ do in the M-stationary case as shown by (2.10). Each of these MTVF processes can be transformed to stationarity using the proper time transformation or by sampling appropriately.

This has been done for processes referred to as $G(\lambda)$ processes in Jiang et al. (2003). These processes are shown to have a frequency structure that changes

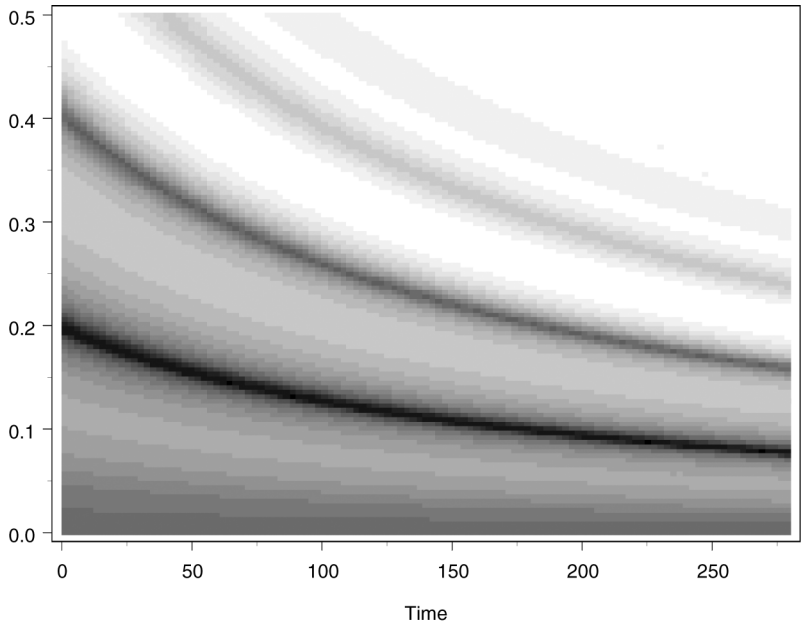

(a) Instantaneous Spectrum

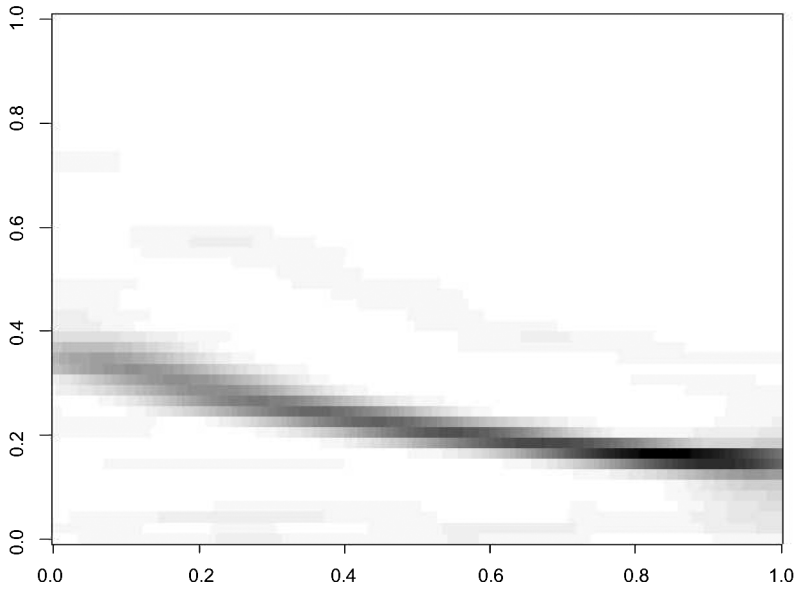

(b) Gabor Transform

Figure 17. Spectral displays for data simulated from Euler(12) model factored in Table 4.

asymptotically like αt^{β} for some α and β. Moreover, if $\lambda = 1$, these processes are the usual stationary processes while if $\lambda = 0$, these processes are M-stationary processes. For $\lambda > 1$ the waveforms contract while for $\lambda < 1$ they expand. A complete development of such processes as well as of linear, quadratic, and exponential

chirp processes will be the topics of several future papers. For a rather complete development of $G(\lambda)$ processes see Jiang et al. (2003). For linear and quadratic chirp processes, see Liu et al. (2004).

8. Concluding Remarks

In this article we have expanded the properties and applications of the discrete M-stationary process introduced by Vijverberg and Gray (2003). The concept of the instantaneous spectrum of an M-stationary process has been introduced in a natural way. Through the instantaneous spectrum we have demonstrated that when the data have a quasi-periodic structure that lengthens approximately linearly in time, the M-spectrum describes the changing frequency with time more accurately than current methods. In current research we have extended these results to the case in which the periodic structure changes like at^{α}, $a > 0$, $-\infty < \alpha < \infty$, as well as to linear and quadratic chirps.

Finally, we should mention that since the equally spaced data from a continuous M-stationary process can be viewed as unequally spaced data from a continuous autoregressive process, one could conceptually avoid interpolation by employing the Kalman filter. However, for the higher-order processes the algorithm may become unstable. The authors are presently examining this approach.

References

Box, G. E. P., Jenkins, G. M., Reinsel, G. C. (1994). *Time Series Analysis: Forecasting and Control.* 3rd *ed.* Englewood Cliffs: Prentice Hall, Inc.

Girardin, V., Rachdi, M. (2003). Spectral density estimation from ran- dom sampling for multiplicative stationary processes. *Computers and Mathematics with Application* 6:1009–1022.

Girardin, V., Senoussi, R. (2003). Semigroup stationary processes and spectral representation. *Bernoulli* 9:857–876.

Gray, H. L., Zhang, N. (1988). On a class of nonstationary processes. *J. Time Series Analy.* 9(2):133–154.

Gray, H. L., Vijverberg, C. P. (2003). Time deformation and the M-spectrum—a new tool for cyclical analysis. Southern Methodist University Department of Statistical Science Technical Report SMU-TR-314.

Herr, A., Klont, N., Atkinson, J. (1997). Identification of bat echolocation calls using a decision tree classification system. *Complexity International*, 4.

Jiang, H., Gray, H. L., Woodward, W. A. (2003). Time varying frequency analysis—G(λ) stationary processes. Southern Methodist University Department of Statistical Science Technical Report SMU-TR-311.

Liu, L., Gray, H. L., Woodward, W. A. (2004). On the analysis of linear and quadratic chirp processes using time deformation. Southern Methodist University Department of Statistical Science Technical Report SMU-TR-317.

Vijverberg, C.-P. C. (2002). Discrete multiplicative stationary processes. Ph.D. Dissertation, Department of Statistical Science, Southern Methodist University.

Vijverberg, C. P., Gray, H. L. (2003). Time deformation and the M-spectrum—a new tool for cyclical analysis. Southern Methodist University Department of Statistical Science Technical Report SMU-TR-314.

Xu, J., Durand, L. G., Pibarot, P. (2000). Nonlinear transient chirp signal modeling of the aortic and pulmonary components of the second heart sound. *IEEE Trans. Biomed. Eng.* 47(10):1328–1335.